AGU100 ADVANCING EARTH AND SPACE SCIENCE

Geochemistry, Geophysics, Geosystems

RESEARCH ARTICLE
10.1029/2018GC007674

Key Points:
- Large-scale submarine landslides observed on open slopes are more likely the composite of smaller scale more frequent slope collapses
- Slides originating from the same source area can display different types of deposits indicating that the flows had different rheologies
- To distinguish separate slide events in a slide complex, an extensive and diverse high-resolution data set is necessary

Supporting Information:
- Supporting Information S1
- Supporting Information S2
- Supporting Information S3
- Data Set S1
- Data Set S2

Correspondence to:
A. Georgiopoulou,
aggie.georg@ucd.ie

Citation:
Georgiopoulou, A., Krastel, S., Finch, N., Zehn, K., McCarron, S., Huvenne, V. A. I., et al. (2019). On the timing and nature of the multiple phases of slope instability on eastern Rockall Bank, Northeast Atlantic. *Geochemistry, Geophysics, Geosystems*, *20*, 594–613. https://doi.org/10.1029/2018GC007674

Received 14 MAY 2018
Accepted 4 DEC 2018
Accepted article online 11 DEC 2018
Published online 1 FEB 2019

On the Timing and Nature of the Multiple Phases of Slope Instability on Eastern Rockall Bank, Northeast Atlantic

A. Georgiopoulou[1,2], S. Krastel[3], N. Finch[1], K. Zehn[3], S. McCarron[4], V. A. I. Huvenne[5], P. D. W. Haughton[1,2], and P. M. Shannon[1,2]

[1]UCD School of Earth Sciences, University College Dublin, Dublin, Ireland, [2]UCD Earth Institute, University College Dublin, Dublin, Ireland, [3]Institute of Geosciences, Christian-Albrechts-Universität zu Kiel, Kiel, Germany, [4]Department of Geography, Maynooth University, Maynooth, Ireland, [5]National Oceanography Centre, Southampton, University of Southampton Waterfront Campus, Southampton, UK

Abstract One of the most challenging tasks when studying large submarine landslides is determining whether the landslide was initiated as a single large event, a chain of events closely spaced in time or multiple events separated by long periods of time as all have implications in risk assessments. In this study we combine new multichannel seismic profiles and new sediment cores with bathymetric data to test whether the Rockall Bank Slide Complex, offshore western Ireland, is the composite of multiple slope collapse events and, if so, to differentiate them. We conclude that there have been at least three voluminous episodes of slope collapse separated by long periods of slope stability, a fourth, less voluminous event, and possibly a fifth more localized event. The oldest event, Slide A (200 km^3), is estimated to be several hundred thousand years old. The second event, Slide B (125 km^3), took place at the same location as slide A, reactivating the same scar, nearly 200 ka ago, possibly through retrogression of the scarp. Slide C (400 km^3) took place 22 ka ago and occurred further north from the other slides. Slide D was a much smaller event that happened 10 ka ago, while the most recent event, albeit very small scale, took place within the last 1,000 years. This study highlights the need to thoroughly investigate large slide complexes to evaluate event sequencing, as seismic studies may hide multiple small-scale events. This work also reveals that the same slide scarps can be reactivated and generate slides with different flow behaviors.

Plain Language Summary When studying large underwater landslides, determining whether what we see in our data was created by one large landslide event or several smaller events is very difficult due to the inaccessibility of the deep sea. But, being able to distinguish between different events and their frequency allows for more accurate risk assessments. Forty years ago, a large landslide was discovered in the northeast Atlantic, on the flank of an underwater plateau offshore of western Ireland. Studies since its discovery have interpreted it as one large event. With present-day technology and a higher resolution data set, we have discovered that it is composed of several landslides. The most recent, but very small and localized event, happened in the last 1,000 years. The one before is happened 10,000 years ago, and it was the size of 680,000 Olympic-size swimming pools. Around 22,000 years ago, a landslide 250 times bigger slid down the slope. Two more similar size events happened more than 200,000 years ago, but the further back in time we go the data resolution gets poorer. We think that the sizes of large underwater landslides found in the world's oceans and lakes may have been significantly overestimated, but their frequency may have actually been underestimated.

1. Introduction

Passive margins are often punctuated by large submarine landslides involving several tens to hundreds of cubic kilometers of sediment affecting thousands of square kilometers of seafloor. Due to resolution limitations of seabed bathymetric and seismic data and depth below seafloor restrictions of shallow coring systems, it is often challenging to distinguish whether such large landslides took place as single large events or as several phases that occurred sequentially over a period of time. Imaged slide scars and slide deposits may be the cumulative effect of several episodes of slope instability in the same location, but this can be especially difficult to determine if there are no obvious crosscutting relationships in the scarps or variable scarp degradation and sediment remolding in the bathymetric data and/or resolvable time in the seismic data between depositional lobes. However, distinguishing between events and being able to calculate the

volumes involved in each episode, together with the interval between discrete failures, are of paramount importance in geohazard risk assessment and in particular in modeling landslide-generated tsunamis. For example, Ward and Day (2001) predicted tsunamigenic waves generated by a potential single catastrophic failure of the west flank of the Cumbre Vieja volcano on La Palma in the Canaries that could transit the Atlantic Basin and arrive at the American coasts with wave heights of up to 8 m. However, Hunt et al. (2011), using sedimentary records, demonstrated that collapses on the northern flank of the adjacent island of Tenerife occurred as separate smaller events. They showed that there is a markedly lower tsunamigenic potential where multistage retrogressive failures occur, even where the time interval between individual failures is very short, in the order of a few days (Hunt et al., 2011).

This study focuses on the Rockall Bank Slide Complex (RBSC), a submarine slide complex which lies on the eastern slope of the Rockall Bank offshore western Ireland, facing NW Europe (Figure 1). Bottom current activity and contourite deposition have been invoked as partially responsible for the slope collapses here (Elliott et al., 2010). Buried basement scarps of the Rockall Bank and contouritic deposition atop the scarps have been suggested to play an important role in slope instability by generating differential compaction and pressure gradients and potentially directing fluid escape toward the seafloor (Georgiopoulou et al., 2013). A study using a traverse of four gravity cores across the RBSC determined with radiocarbon dating that sliding took place during the last glaciation (~21.7 ka; Øvrebø et al., 2005). Georgiopoulou et al. (2013) suggested that the RBSC probably occurred as a multiphase slope collapse involving at least three episodes, with a potentially incipient or aborted fourth episode. That study relied on indirect evidence from legacy 2-D seismic reflection and the INSS (Irish National Seabed Survey) bathymetric data from the scar area. In this paper we use the same bathymetric data set, but we combine it with newly acquired sediment cores, radiocarbon ages, and newly acquired 2-D seismic data from further downslope, in the depositional area of the complex to test the hypothesis of Georgiopoulou et al. (2013) and distinguish the different slide episodes, evaluate the volumes involved in each, and determine their timing and recurrence interval.

2. Regional Setting

Rockall Trough is an elongate, steep-sided, NNE-SSW trending intracontinental sediment-starved basin located west of Ireland and the UK (Figure 1). It is 200–250 km wide, with water depths ranging from nearly 3,000 m in the northern part to over 4,000 m in the south where it opens to the Porcupine Abyssal Plain (Figure 1).

To the west, Rockall Trough is bounded by Rockall Bank, a structural high with an almost flat plateau (0–2° slope) at $<$200- to 400-m water depths; Rockall Bank slopes to the east down to 2,400 m in less than 90 km with gradients of 5–10°, in places exceeding 15° (Figure 1).

The Irish continental margin lies at the boundary between the glaciated and the glacially influenced sectors of the European Atlantic margin (Weaver et al., 2000). During the last glaciation the British Irish Ice Sheet (BIIS) was covering the entire island of Ireland and, at the Last Glacial Maximum, 24 ka, it extended and was grounded close to the shelf edge (Peters et al., 2016). Retreat of the ice margin began at 22 ka, but the ice shelf persisted for the next 2,500 years (Peters et al., 2016).

Deep water masses in Rockall Trough flow northward along its eastern margin, deflecting anticlockwise at the steepening slopes of the Wyville Thomson Ridge and there flowing southward along the base of the Rockall Bank, excavating a moat at the base of slope (Figure 1). Bottom currents are responsible for the redistribution of sediments forming sediment drifts, most notably the Feni Drift that occupies the western side of the trough (Figure 1) and is mostly active during interglacial periods (Stoker, 1998; Stoker et al., 1998).

The floor of Rockall Trough is relatively smooth, gently getting deeper toward the southwest. Major depositional processes that have dominated Rockall Trough are the following: the late Miocene to early Pliocene contouritic Feni Drift; the Neogene to Pleistocene glaciogenic Donegal-Barra Fan (DBF), a glacial trough mouth fan that drained the BIIS and occupies the northeastern margin, with depositional lobes that extend toward the deeper parts of the Rockall Trough basin; the RBSC that occupies the northwestern margin and truncates the Feni Drift and interacts with the DBF lobes; and a series of channels that dissect the Irish slope but were mostly active during glacial times (Elliott et al., 2010; Sacchetti, Benetti, Georgiopoulou, et al., 2012;

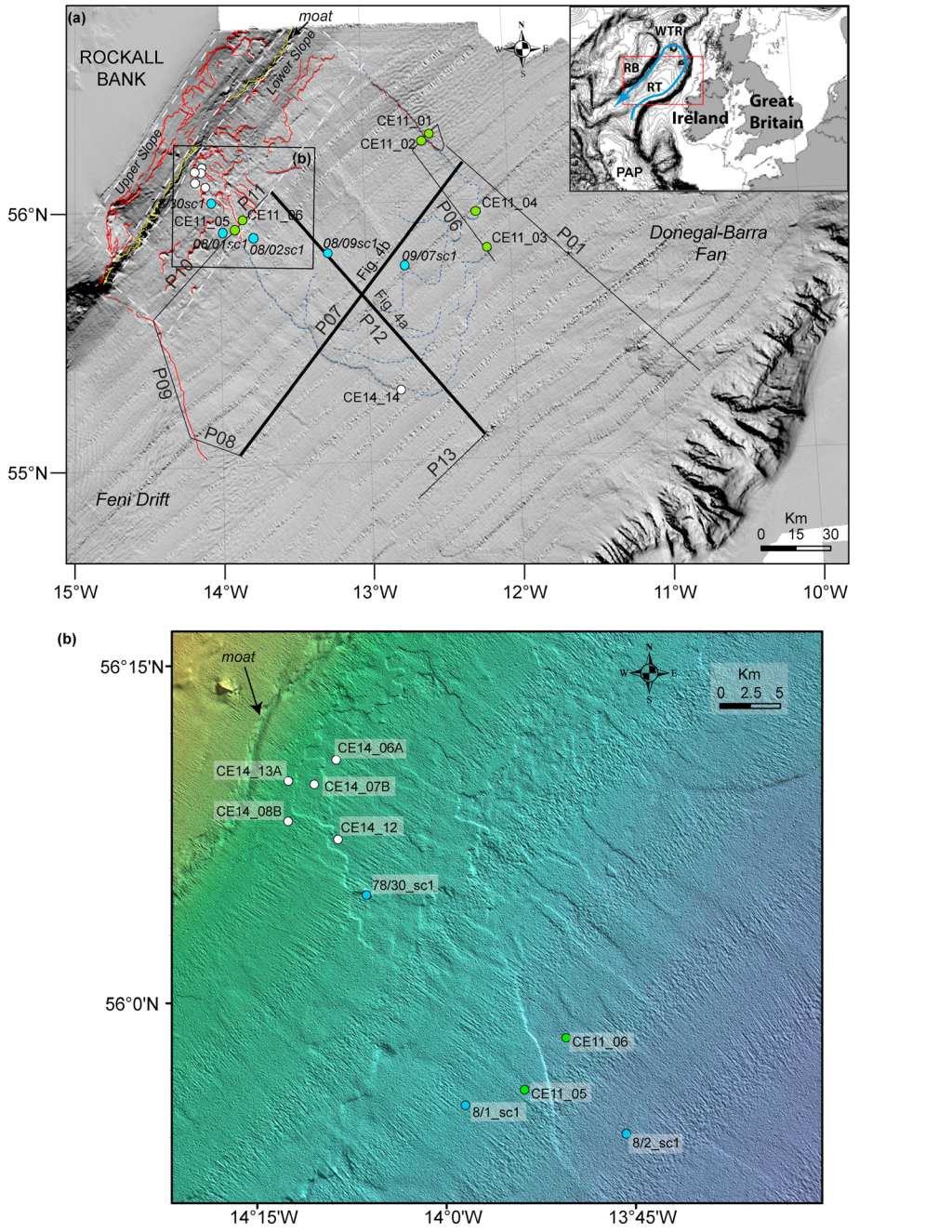

Figure 1. (a) Shaded relief bathymetry map of the northern Rockall Trough offshore western Ireland and data used in this study. The seismic profiles are shown in black and are numbered P01–P13. The locations of CE11011 cores are indicated with green circles and of the CE14011 in white circles. The turquoise circles show the locations of the Øvrebø et al. (2005) study. The red lines show scarps associated with the RBSC, the yellow lines scarps associated with the moat, and the blue dashed lines depict the depositional lobes. The white dashed boxes indicate the Upper and Lower Slope regions after Georgiopoulou et al. (2013). PAP, Porcupine Abyssal Plain; RB, Rockall Bank; RT, Rockall Trough; WTR, Wyville Thomson Ridge. (b) A zoom in bathymetric map on the location of the lower slope scarps and cores. Bathymetric data from the Irish National Seabed Survey program.

Sacchetti, Benetti, Quinn, et al., 2012; Stoker et al., 1998). Shallow cores from the deeper basin floor contain coarse sandy turbidites and contourites alternating with hemipelagic layers (Georgiopoulou et al., 2012). Turbidite provenance analysis suggests a switching of sources across the glacial-interglacial transition, with turbidites coming from the Irish margin during the last glacial, via the DBF and the Irish slope channels,

probably generated by meltwater, and then, from Rockall Bank during the current interglacial, potentially as flow transformation products from the Rockall Bank slope collapses (Georgiopoulou et al., 2012). The glacial hemipelagic intervals show the characteristic influence of ice-rafted debris (Georgiopoulou et al., 2012).

Sedimentation rates were as high as 17.1 cm/ka during the Holocene on the crest of the Feni Drift but were lower (14.6 cm/ka) during the last glacial period, and significantly less prior to that, averaging 5 cm/ka for the Pleistocene (van Weering & de Rijk, 1991).

The RBSC truncates a field of sediment waves associated with the Feni Drift (Figure 1). It also excavated part of Rockall Bank and deposited sediment onto the floor of the trough (Elliott et al., 2010; Flood et al., 1979; Georgiopoulou et al., 2013; Unnithan et al., 2001; Figure 1). Scarps associated with the RBSC have regional average gradients 30–35° and locally up to 70° (Georgiopoulou et al., 2013). Volumes excavated from the entire scar have been estimated to be between 260 and 760 km^3 (Georgiopoulou et al., 2013). The glide plane for the RBSC is believed to be the regional intraearly Pliocene C10 unconformity (Elliott et al., 2010). The sedimentary sequence between C10 and the present-day seafloor outside of the main area of failure (RTa in Stoker et al., 2001) comprises alternating debris flow deposits and parallel- to wavy-bedded drift accumulations, locally disrupted by slope failure deposits (Stoker et al., 2001).

3. Data and Methodology

Our study is based on 13 new multichannel high-resolution seismic profiles (a total of approximately 700 line-km), six new piston cores collected during RV Celtic Explorer cruise CE11011, five new gravity cores collected during the SORBEH (Slope Collapses on Rockall Bank and Escarpment Habitats) CE14011 expedition, four gravity cores from Øvrebø et al. (2005), and open-access bathymetric data that had been acquired as part of the INSS program between 2000 and 2001 on RV Bligh (Figure 1). The multibeam bathymetry was collected using a Simrad EM120 multibeam echo sounder with frequencies of 11.75–12.75 kHz. A detailed account on the processing of the multibeam data can be found in Sacchetti, Benetti, Quinn, et al. (2012).

The seismic source used for acquiring the seismic data was a Mini-GI Gun. The gun was shot in true GI-Gun mode with a volume of 0.2 L for the generator and 0.4 L for the injector. The dominant frequency is ~200 Hz. The injector was triggered with a delay of 20 ms after the generator to suppress the bubble signal in the recorded seismic data. The shooting rate was 9 s resulting in a shot point distance of ~20 m at 4.5 knots boat speed. The gun operation employed a high air pressure of 150 bar (2150 PSI). The data were received by a 187.5-m-long 120-channel streamer (Geometrics GeoEel); channel spacing was 1.56 m. Positioning was based on GPS (Global Positioning System).

The processing procedure included trace editing, setting up geometry, binning at 5-m bin distance, static corrections, normal moveout corrections, filtering, stacking, and finite difference time migration. A common midpoint spacing of 5 m was applied throughout. A constant velocity of 1,500 m/s was chosen for the NMO correction and migration as the streamer was too short for a velocity analysis. Poor weather conditions during acquisition caused a relatively high noise level in the data, but the careful data processing allowed to produce images with a good signal-to-noise ratio. All seismic profiles are available in Supporting Information S1. The average depth of penetration was 0.5 s, but the signal is very attenuated beyond 0.3 s. With a sediment velocity of 1,800–2,000 m/s the vertical resolution within those top 0.3 s is approximately 2.5 m. Seismic reflections were picked and interpolated to produce surface maps in Kingdom Suite. The gridding algorithm selected was Flex Gridding.

New cores from two different cruises are combined in this study (Supporting Information S3). The CE11011 (CE11) cores were collected using a Geo-piston corer with 110-mm-diameter and 6-m-length barrels. Six cores were collected (Figure 1) with average retrievals of 3.5 m, with the longest retrieval being 4.29 m below the seafloor. The CE14011 (CE14) cores were collected using a 65-mm-diameter gravity corer with 3- and 6-m-long barrels and average retrieval of 1 and 1.9 m respectively.

The cores were first described visually for sediment structures, grain size, and color (Supporting Information S2). They were then logged for physical properties (gamma ray, *P* wave velocity, magnetic susceptibility, and lightness) in a GeoTek Multi-Sensor Core Logger in split mode setup in the Irish Sediment Core Research Facility at Maynooth University (Supporting Information S4). Selected sandy samples were examined under a binocular microscope for bulk mineralogy comparisons of different sandy intervals.

Table 1
Raw Radiocarbon Data, Calibrated Ages, and Resulting Sedimentation Rates

Core	Depth downcore (cm)	Age ^{14}C (BP)	Calibrated (BP)[a](min-max)	Calibrated (BP; average)	Postglacial sedimentation rates (cm/ka)
CE11_02	210	15,200 ± 80	17,670–18,197	17,940 ± 260	11.7
CE11_03	10	2,165 ± 30	1,545–1,838	1,690 ± 150	2.45
CE11_03	22	7,360 ± 40	7,643–7,915	7780 ± 140	
CE11_03	42	13,010 ± 70	14,310–15,161	14,740 ± 430	
CE11_05	73	24,960 ± 190	28,049–28,941	28,500 ± 450	2.56
CE11_06	134	13,830 ± 70	15,806–16,333	16,070 ± 260	12.3
CE11_06	203	18,420 ± 100	21,420-22,087	21,750 ± 330	
CE14_07A	65	10,160 ± 50	8,941–9,268	9,120 ± 178	7.12
CE14_07A	129	19,590 ± 170	20,630–21,555	21,092 ± 462	samples bracket an erosional event
CE14_07A	156	25,020 ± 190	26,160–27,096	26,614 ± 454	
CE14_08B	20	19,150 ± 110	20,389–20,933	20,661 ± 272	sample within debrite clast
CE14_08B	40	>46,000			
CE14_08B	64	>46,000			
CE14_08B	64	>46,000			
CE14_08B	187	>46,000			
CE14_08B	192	>46,000			
CE14_08B	237	>46,000			
CE14_12	69	20,400 ± 120	21,697–22,378	22,037 ± 340	3.13
CE14_12	121	>46,000			
CE14_12	162	>46,000			
CE14_13A	29	9,820 ± 50	8,550–8,969	8,760 ± 209	3.3
CE14_13A	64	20,590 ± 120	21,928–22,569	22,248 ± 320	under erosional event
8/9_sc1	90	9,500 ± 55	10,099–10,305	10,202 ± 103	8.82
8/9_sc1	120	>46,000			
9/7_sc1	160	20,540 ± 140	23,317–24,189	23,753 ± 436	6.75
9/7_sc1	200	18,800 ± 120	21,383–22,106	21,744 ± 361	under erosional event

Note. Calibration Stuiver et al. (1998).
[a]delR = 53 ± 50.

A total of 23 samples were taken for radiocarbon AMS (^{14}C) dating and are supplemented by three more from Øvrebø et al. (2005) (Table 1). The analysis was performed on pristine planktonic foraminifera shells of mixed species as there was very little material for monospecific picking. The dating was performed by the Poznań Radiocarbon Laboratory. The results were calibrated using Calib v7.0.4, based on the Marine 13 calibration data set (Reimer et al., 2013; Table 1). A marine reservoir correction was applied based on data from the nearest location of δR = 53 ± 50 (Castle Rock, North Channel; Harkness, 1983). Sedimentation rates are calculated between two samples taken from the same core or, where only one sample was taken from the core, between the top of the core taken to be Present Day, that is, 0 years before present (BP) and the depth of the sample. This was possible as there is no evidence of erosional features, no significant event beds or major facies changes between the sample depths, and we are confident that the seafloor was recovered, usually obvious by the characteristic orange hue of oxidation.

Between the lower two samples of CE14_07A there is a debrite; therefore, no sedimentation rate between those two samples was calculated.

The top sample of CE14_08B was aiming to sample the base of a turbidite, but it appears to have sampled a clast of the underlying debrite; therefore, it is not used to calculate a sedimentation rate.

The sample from CE14_13A at 64 cm dates the hemipelagic sediment at the base of a turbidite, which was likely erosional; therefore, it is not used to calculate a sedimentation rate.

Attributed by Ovrebo either to bioturbation or muddy turbidite.

4. Results and Interpretation

4.1. Bathymetry

The planform morphology of the RBSC has been described in several previous studies (Elliott et al., 2010; Flood et al., 1979; Georgiopoulou et al., 2013; Sacchetti, Benetti, Quinn, et al., 2012), so only a brief

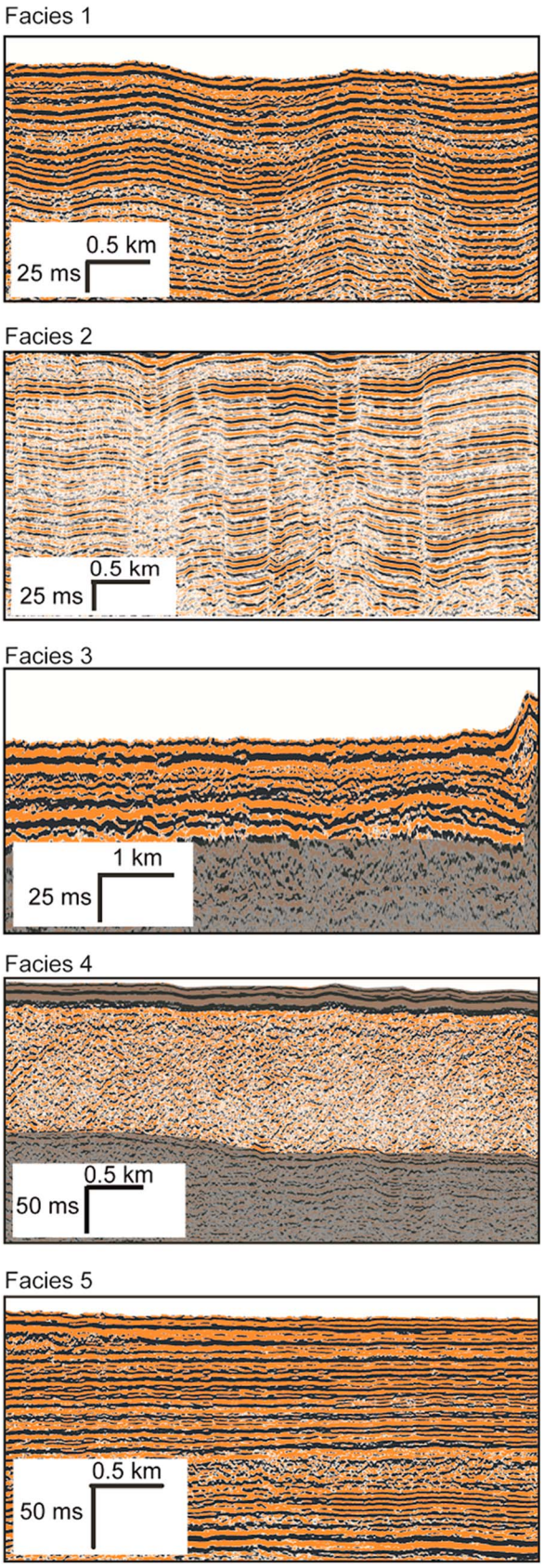

Figure 2. Seismic facies identified on the 13 seismic profiles.

summary is provided here with an emphasis on the lower slope and insights from the newly acquired seismic data. On the basis of different degrees and styles of deformation, the upper slope, where the scars of the RBSC are found, was divided into the Upper slope region and the Lower slope region, which are separated by an alongslope moat that strikes parallel to the base of slope at approximately 1,500-m waterdepth (Georgiopoulou et al., 2013). The Upper slope region was further subdivided into the North, Central, and South regions, which demonstrate very different scarp characteristics; the North has rough-edged, arcuate scarps up to 150-m high, whereas the South is dominated by cuspate, bite-shaped, smooth-edged scarps also up to 150-m high (Georgiopoulou et al., 2013). Strikingly different is the Central area, where there are at least three scars, much shallower, up to 20-m high, separated by flat-topped ridges (Georgiopoulou et al., 2013). The total width of the upper slope area that is affected by scarps is 120 km (Figure 1).

Less than 5 km downslope of the moat, the Lower slope region is severely scarred by multiple intersecting scarps (Figure 1; Georgiopoulou et al., 2013). Here the RBSC is clearly still erosional and its margins are defined by truncations of the sediment wavefields of the Feni Drift, along the south and the north sidescarps (Figure 1). Cores CE11_01 and CE11_02 have targeted the northern sidescarp, with CE11_01 serving as a reference core from the undisturbed seafloor and CE11_02 taken inboard of the scarp (Figure 1a). There are a number of other sidescarps within this area, downslope of the Lower slope region. Planar terraces at different stratigraphic levels can be identified here, and we observe a flow fabric downslope from them with elongate linear furrows, ridges defining a conical-shaped erosional region opening downslope (Figure 1b). The CE14 cores targeted these terraces (Figure 1b).

In the distal/depositional area the seafloor is occupied by a set of overlapping lobes, which at the toe of the complex have sharp, up to 25-m high, frontal margins. Cores CE11_03, CE11_04, and CE14_14 have targeted the terminations of these lobes (Figure 1).

4.2. Seismic Facies and Their Distribution

The newly acquired multichannel seismic profiles provide a higher resolution of the subseafloor sequence than previously seen on the legacy industry seismic profiles (e.g., Elliott et al., 2010; Georgiopoulou et al., 2013). The new data reveal that the acoustic character of the sediments is highly variable both laterally and vertically. Five seismic facies have been identified and mapped based on this newly acquired data set (Figures 2 and 3).

1. Facies 1 comprises parallel, wavy, continuous reflections of moderate to strong amplitude. The wavelength is between 1 and 2.6 km and the amplitude 5–10 m. This facies, consisting of interbedded lithologies giving it its characteristic *striped* appearance, is interpreted as the deposits of sediment waves created by bottom currents. Their distribution coincides with sediment waves interpreted previously from bathymetric and seismic data (Elliott et al., 2010; Sacchetti et al., 2011; Sacchetti, Benetti, Quinn, et al., 2012), while the scale range of approximately 1-km wavelength and 20-m height generally agrees with the size of bottom current-related sediment waves (Wynn & Stow, 2002). The sediment waves are part of the Feni

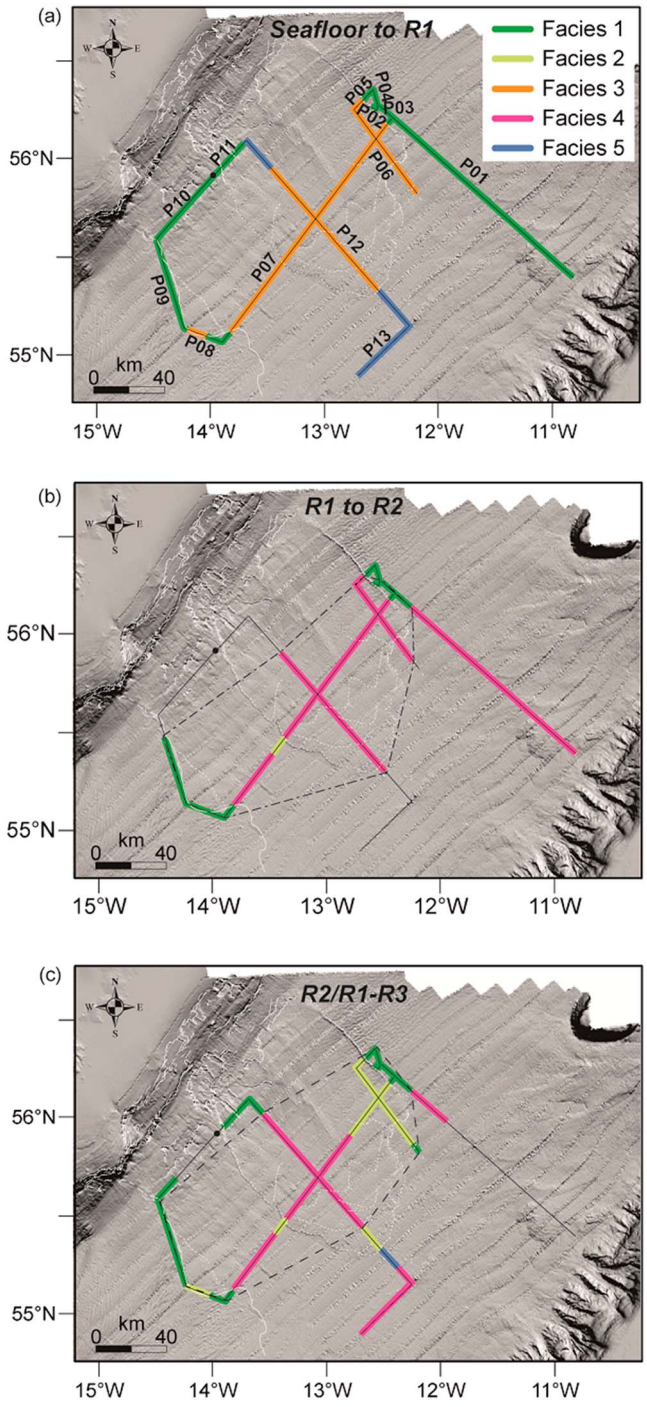

Figure 3. Distribution of the seismic facies on the profiles at different stratigraphic levels. The thin white lines show the scarps and depositional lobes of the Rockall Bank Slide Complex. (a) Between the seafloor and Reflector 1, (b) between Reflector 1 and Reflector 2, and (c) between R2 (and where it missing R1) and reflector R3. The dashed and dotted line in (b) and the dashed line in (c) show the mapped extent of R2 and R3, respectively (see also Figure 5).

contourite drift and are sharply truncated by the RBSC scarps (Faugères et al., 1999; Flood et al., 1979; Sacchetti et al., 2011).

2. Facies 2 is characterized acoustically by weak to moderate amplitudes and contains parallel semicontinuous reflections. We interpret this facies also as generated by sediment waves but within the scarps in the northern RBSC-affected area in the deeper sedimentary sequence (Figure 3c), which explains the weakening of the seismic amplitude. They are sharply truncated to the southwest by a scarp. This relationship has implications on the timing of the RBSC events and will be discussed further in section 4.5.
3. Facies 3 shows subparallel, partly discontinuous, irregular reflections with high amplitudes. We interpret facies 3 sediments as draping hemipelagic sediments, possibly punctuated by turbidites, healing the topography left by the RBSC, as in most cases it is found covering facies 4.
4. Facies 4 is acoustically chaotic to transparent with few discernible structures or reflections. Facies 4, which occupies mostly areas within the RBSC limits (scarps and lobes) near the surface and at depth, represents deformed slope sediments. The acoustic character demonstrated in this facies (transparent, chaotic reflections) is typical of slide deposits (e.g., Bull et al., 2009; Sacchetti, Benetti, Georgiopoulou, et al., 2012). The extent of this seismic facies suggests that slide deposits are present beyond the confines of the RBSC limits as seen on the seafloor, to the east (Figure 4). This is coincident with the southwestern reaches of the glacially fed DBF that is sourced from the northeast Rockall Trough margin and is almost entirely composed of debrites and mass transport deposits (Georgiopoulou et al., 2012; Holmes et al., 1998; O'Reilly et al., 2007; Sacchetti et al., 2011).
5. Facies 5 shows parallel, mostly continuous reflections of high amplitude. Facies 5 is similar to facies 1 in that it is characterized by a continuous layered seismic character. However, it lacks the undulating character of facies 1. On the other hand, given the similarity of the acoustic character, the lithologies are likely to be similar to those of facies 1 and similarly with facies 3 are interpreted as hemipelagic sediments with interbedded turbidites. Sediment cores from the near surface that have been collected in the area of facies 5 distribution confirm the presence of intercalated hemipelagic sediments with sandy turbidite beds (Georgiopoulou et al., 2010; Georgiopoulou et al., 2012).

Three seismic horizons (R1–R3) have been mapped on most seismic profiles (Figure 4), based on their spatial continuity and their positioning relative to the acoustic facies distribution. Horizon 1 (R1) defines the surface postfailure sediments and has been mapped about 20–30 ms below the seafloor throughout the survey. R1 is mostly continuous, only in places patchy, with low-to-moderate amplitude. R1 is widespread and could be mapped on all profiles (Figure 5a). The surface sediments that lie between R1 and the seafloor are mostly high-amplitude, continuous reflections of facies 1 and 5 outside the RBSC sidescarps, and mostly facies 3 within the scarps (Figure 3a), with the exception of an area of facies 1 that stretches within the scar near the base of slope, along profiles P10 and P11 (Figure 3a).

Horizon 2 (R2) is a moderate-amplitude, continuous reflector that is found in the central and northern part of the survey (Figure 5b). It is less widespread than R1, with clear terminations within the study area; it shallows

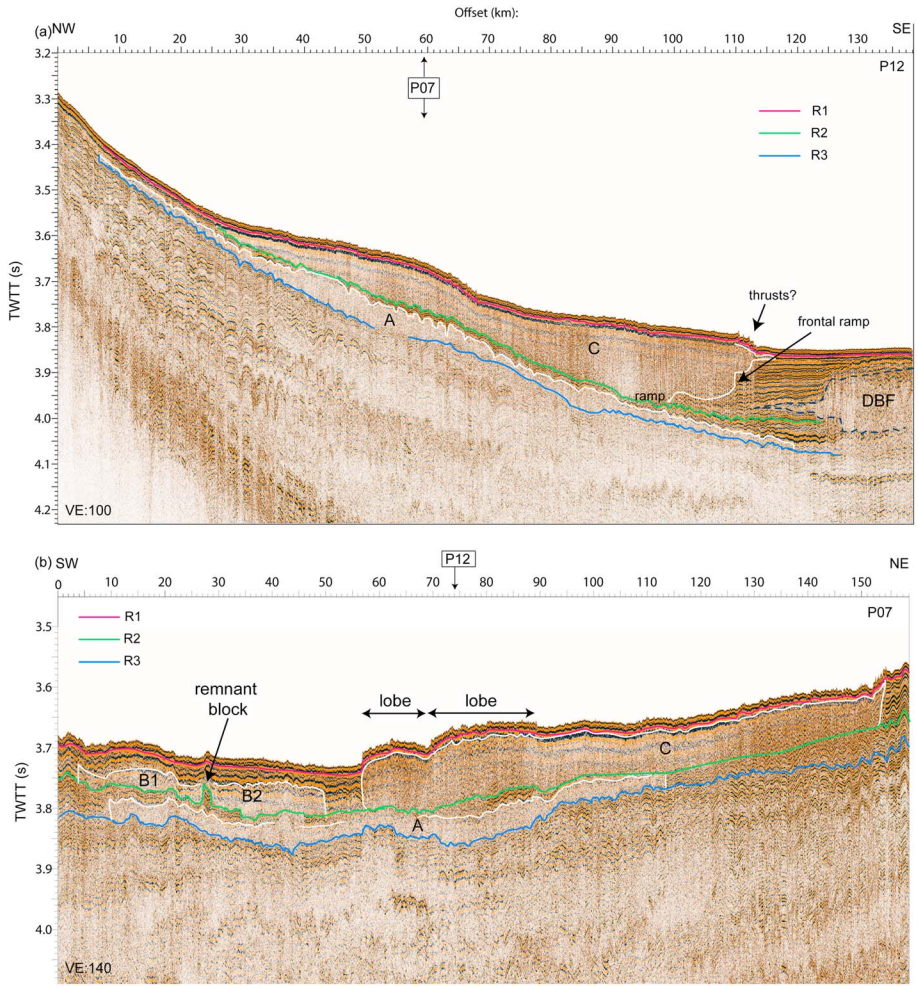

Figure 4. Seismic profiles (a) P12 along the length of the Rockall Bank Slide Complex lobes and (b) P07 across the Rockall Bank Slide Complex lobes (for location see Figure 1). Reflectors R1–R3 are shown in magenta, green, and blue, respectively. The white lines are showing the upper and lateral limits of slide bodies A, B1, B2, and C. The profiles cross where indicated in each figure with an arrow.

upslope and downslope toward R1 (Figure 5b) and is sharply truncated on profile P01 (Supporting Information S1). Between R1 and R2 the most prevalent facies is facies 4, at least within the RBSC affected area, where it pinches out both upslope and downslope (Figure 3b). Outside the sidescarps,

facies 1 is continuous from the seafloor down to the level of R2 and below (Figure 4b). Facies 4 is also found beyond the RBSC-affected area as seen on profile P1, which traverses the depositional lobes of the Donegal Barra Fan (Figures 3b and 3c).

Horizon 3 (R3) is an irregular, moderate amplitude reflector that is fairly continuous and mapped throughout most of the survey (Figures 4 and 5c). On profile P12 the quality of the seismic deteriorates southeastward and it is impossible to map the reflector. On profile P01 R3 is abruptly truncated against facies 4 (Supporting Information S1). Facies 4 and 2 are found between R3 and R2; facies 4 is located primarily in the central and southern area and facies 2 in the northern edge, against the northern sidescarp (Figure 3c). Outside the limits of the RBSC, facies 1 continues to be dominant in the R2–R3 interval (Figure 3c).

4.3. Sedimentary Facies

The core data allow us to identify five main sedimentary facies. The criteria used are color, foraminifera content, sedimentary structures, and physical properties (Figure 6).

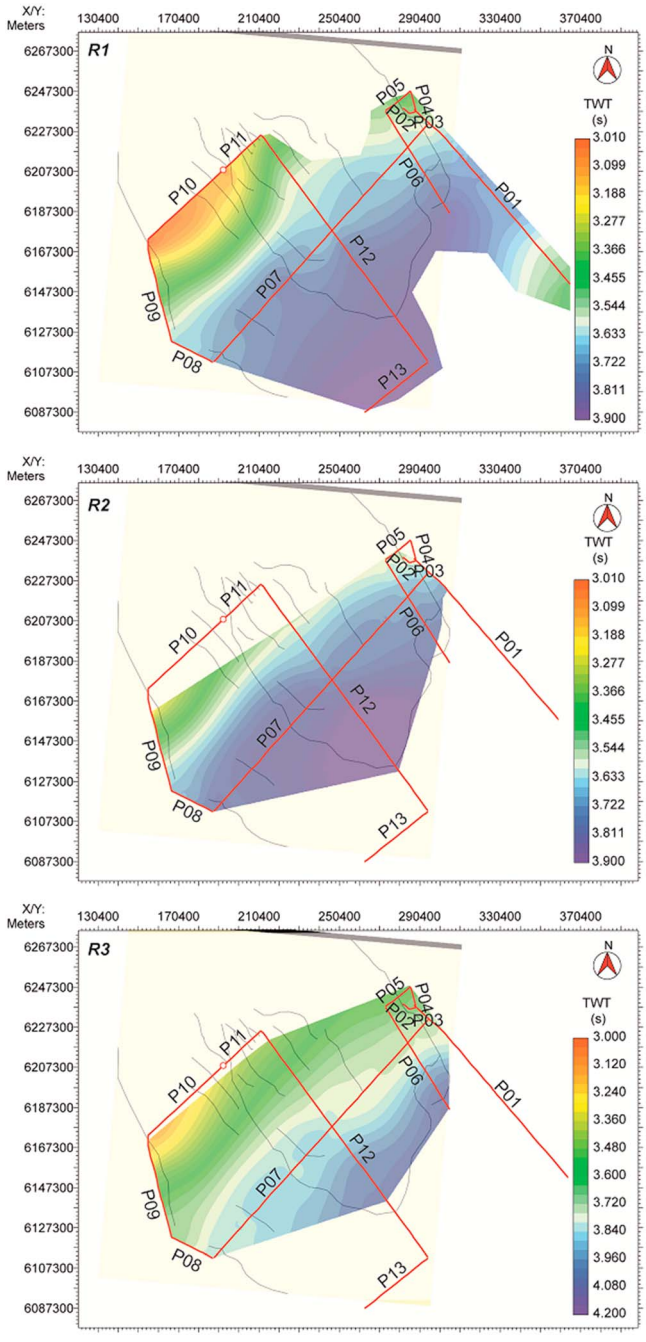

Figure 5. Maps of the three reflectors. Note (a) the widespread distribution of R1 in and (b) the limited distribution of R2 relative to both (a) R1 and (c) R3.

HM are muds, further divided into two subfacies; HM1, a light-colored silty, foraminifera-bearing mud; and HM2, a dark-colored, mottled, foraminifera-poor, clayey mud. Their physical properties do not differ much; they show only very subtle differences in *P* wave velocity and gamma-ray density, while magnetic susceptibility seems to be higher in HM2. Both subdivisions of Facies HM are found in all cores (Figure 7).

CD are clast-supported debrites and can be found in cores CE11_05 and CE11_06, CE14_12, _13A, and CE14_06A and cores 8/9sc1 and 78/30sc1 (Figure 7a).

Facies SD represents deformed layers that may be sheared, folded, or disrupted. For example, there is a section of CE11_03, between about 80- to 175-cm downcore, which appears deformed (Figure 7b). The deformation cannot be attributed to coring

problems as it is not pervasive. However, it does not appear to be disintegrated and mixed as it maintains the original structures which in this facies appear deformed.

ST are sandy layers (fine to medium sand), often fining upward. In several of the cores this facies sits directly on top of CD. In most cases, the sandy layers appear laminated, better visible in the X-rays (Figure 6). Where lamination is not present the layers appear disturbed and fluidized, which may suggest destruction of the original structures, possibly because of coring (Jutzeler et al., 2014). They are characterized by increases in *P* wave velocity, gamma-ray density, and magnetic susceptibility (Figure 7).

TB are thinly bedded silt-fine sand layers in dark clayey mud background (Figure 6). Facies TB is only seen in cores near the axis of the trough CE11_03, CE11_04, and CE14_14 but is significantly thicker in CE11_03 (Figure 7a). In this interval, the physical properties, particularly the gamma-ray density and magnetic susceptibility, appear erratic, but the pattern seems to suggest increases for both parameters in the coarser layers (Figure 7a).

We interpret facies HM as background hemipelagic sediments with different degrees of bioturbation, mostly by Zoophycos. The two subdivisions, HM1 and HM2, are similar to the GM and BM facies reported in deeper water by (Georgiopoulou et al. (2012). Like that study, and based on radiocarbon dating (Figure 7), we interpret HM1 to represent sediments deposited during the current interglacial, which explains the higher foraminifera content and the light color, indicative of higher carbonate content and therefore higher productivity. The darker muds with the black staining and paucity of foraminifera were deposited during the last glacial, confirmed also by the dating (Figure 7). The age of the transition from the last glacial to the current interglacial according to the radiocarbon data is 13 ka (based on CE11_03). We attribute that the high degree of bioturbation through HM1 is attributed to interglacial burrowing activity as evidenced by the light grey HM1 mud that has been mixed with the darker HM2 mud.

Facies TB can be found only in CE11_03, CE1 _04 and CE14_14, which are the cores closest to the axis of the Rockall Trough and nearest the Irish margin (Figure 1b). We interpret this facies as fine grained-turbidites originating from meltwater plumes from the BIIS that was covering the Irish shelf to the east of the study area at the time (Peters et al., 2016). They correspond to the turbidites that are found as thicker and slightly coarser sequences in cores more proximal to the Irish slope (Georgiopoulou et al., 2012), but they are not found in cores closer to Rockall Bank. Rockall Bank was likely too distal for these turbidity currents and is also in shallower waters.

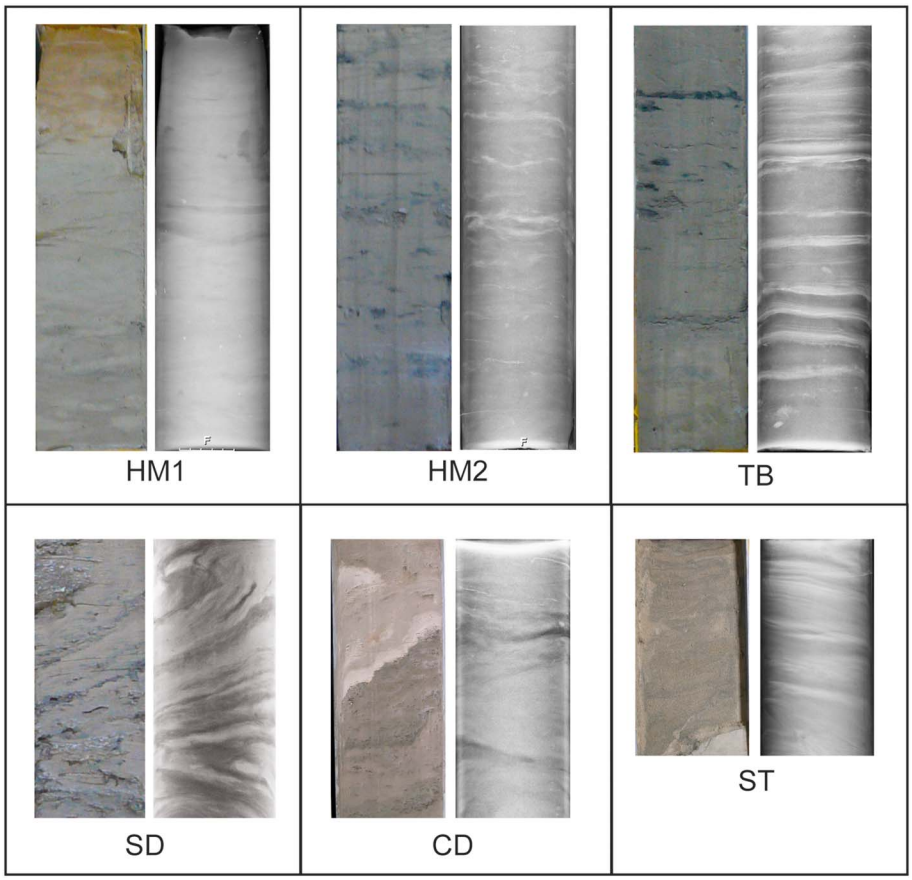

Figure 6. Sedimentary facies identified in the cores. Photo on the left and X-ray on the right for each of the sedimentary facies. See text for more details.

The clast-supported character of facies CD indicates that this is a debrite composed of clasts of multiple lithologies. This is the same character as reported by (Faugères et al., 1981; Øvrebø et al., 2005).

The section 83–240 cm in CE11_05 that corresponds to facies SD is remarkably different when compared with the interval immediately below it in that it is not composed of multiple clasts. Instead it appears similar to the glacial background sediments, but the bioturbation is deformed there are some small (1- to 2-cm diameter) clasts floating in the mud, and the X-rays show sheared and inclined layers (Figure 7a). These two sections could either be interpreted as two debrites that are stacked or infer that the interval 83–240 cm is a larger clast within the debrite. We prefer the second interpretation as there is no sharp change in the gamma-ray density log (Figure 7a), where the second debrite would be shearing and depositing on top of the older one, causing compression and/or eroding into deeper-buried strata with increased density.

The debrite is capped by facies ST in CE11_05 and CE11_06 (Figure 7a). We interpret this to be a cogenetic turbidite that deposited from a more dilute suspended flow through debris flow transformation or mobilized at the same time as the debris flow. This relationship was also observed in the nearby gravity core 08/09sc1 of (Øvrebø et al., 2005). However the ages of the deposits do not match (Figure 8) and therefore cannot be correlated. They also correlate with the debrite near the bottom of CE14_07A and the one in CE14_12 (Figures 7a and 8). About 30 km laterally toward the east, neither the debrite nor the turbidite can be correlated into CE11_03 and CE11_04, but stratigraphically they coincide with the top of the disturbed sequence in CE11_03 (Figures 7b and 8). This suggests that either the flow ceased close to the location of 09/07sc1 or that it carried on beyond that location but just did not expand laterally toward the east. Debrite/turbidite events occupying cores CE14_08B and 78/30_sc1 are difficult to correlate with any of the other events and may represent a separate single event.

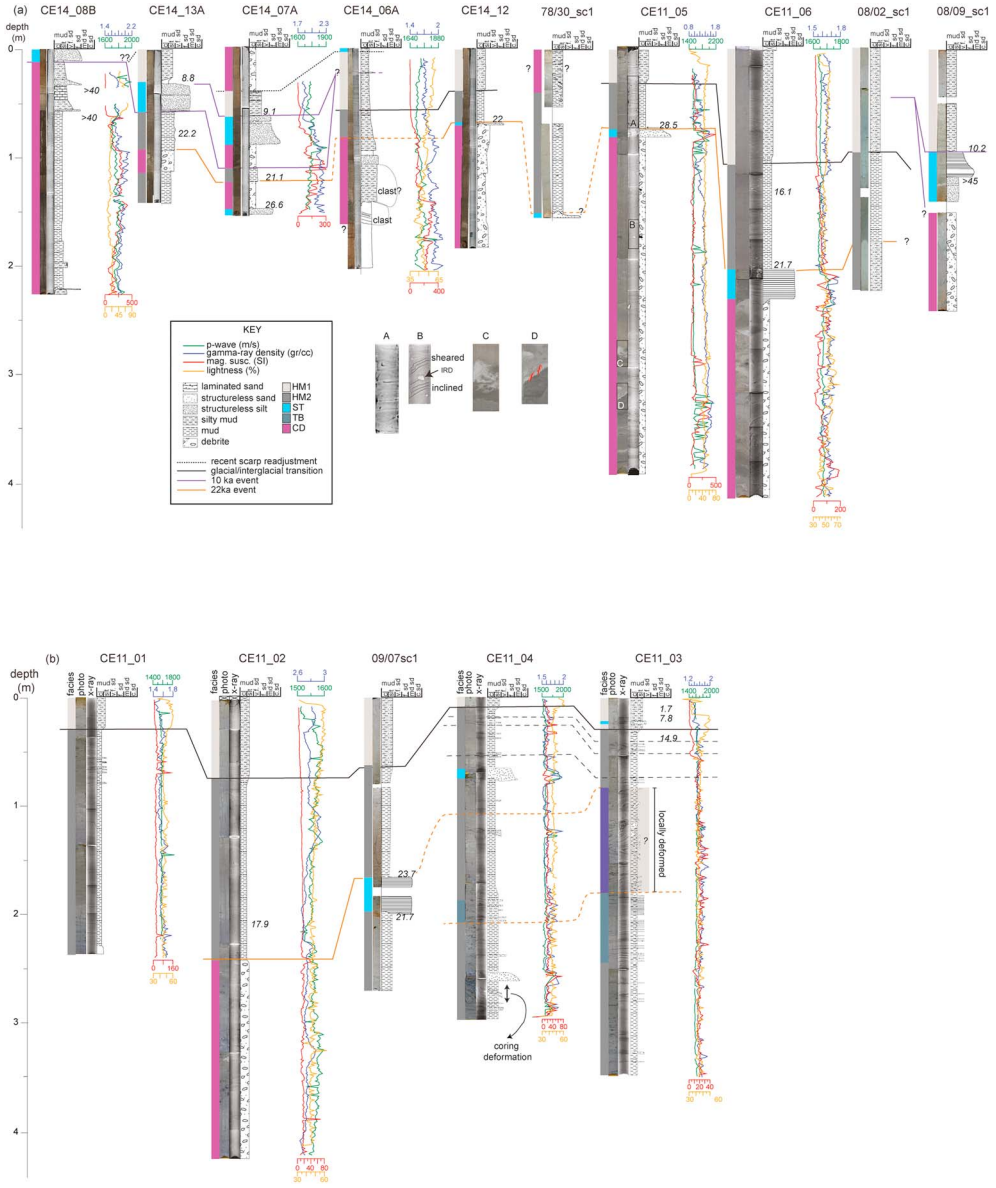

Figure 7. (a) Correlation panel of the lower slope cores, parallel to the flow axis; (b) correlation panel of the cores along the northern edge of the Rockall Bank Slide Complex. For each core we show the photo, X-ray (where available), lithological log, facies interpretation, and physical properties (where available). The solid lines show confident correlations, whereas dashed lines are inferred correlations and extensively discussed in the text. The ages (italics) are shown in years BP. Insets A–D are blowups of the photo and X-ray from core CE11_05 and show in more detail the internal deformation in the debrite. Note the very small increase in density at 240-cm downcore in CE11_05; if two separate debrites were stacked the density at their contact would be expected to show a significant increase to the right. The coring disturbance indicated in core CE11_04 took place during extraction of the core from the barrel.

The timing of emplacement of these debrites and turbidites is discussed further in section 4.5.

4.4. Sedimentation Rates

Sedimentation rates were calculated in intervals of hemipelagic sediments that are not punctuated by any deposits that might have been erosional. Therefore, not all radiocarbon dates were used (Table 1).

CE11_03 and CE11_05 show relatively slow sedimentation rates (ca 2.5 cm ka^{-1}) compared to CE11_06 and CE11_02 (both about 12 cm ka^{-1}; Table 1). We believe these differences can be attributed to the location of

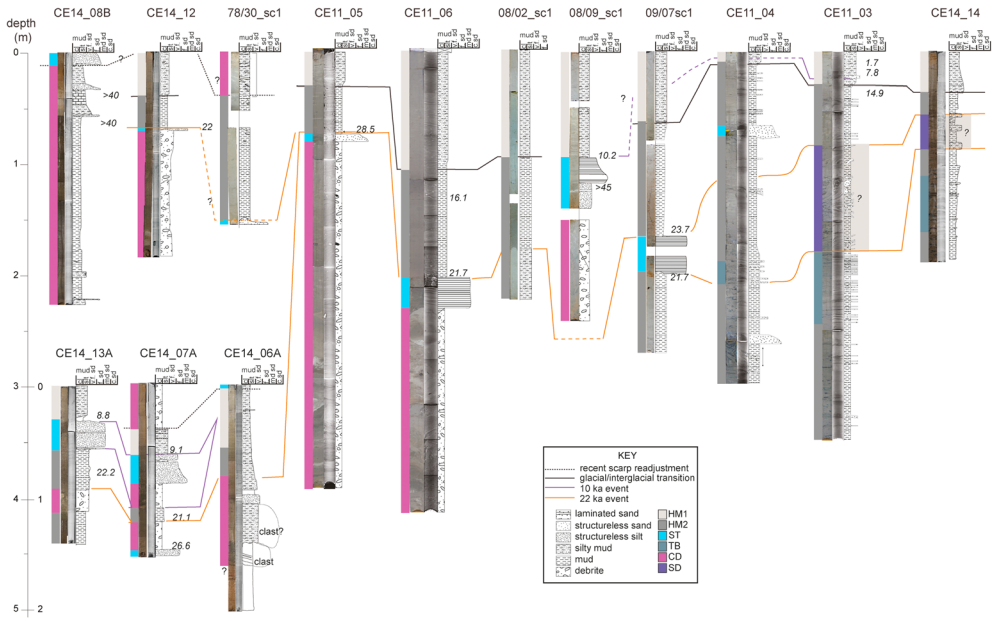

Figure 8. Correlation panel of all the cores used in this study as compiled from Figures 7a and 7b.

the cores relative to the route of the bottom current, suggesting that our cores straddle the boundary of the deep water mass that sweeps the base of slope of Rockall Bank. Where the current effect exists, the sedimentation rates are larger, i.e., where cores CE11_02 and CE11_06 were taken from, as opposed to the location of CE11_03 which is beyond the effect of the bottom current. This interpretation is further corroborated by the presence of sediment waves around CE11_02 and CE11_06, but not around CE11_03 (Figure 1). A problem that arises with this interpretation is that CE11_05 was taken only 5.5 km away from CE11_06, and yet the sedimentation rate is nearly an order of magnitude lower. Three reasons can be invoked to explain this difference; (1) the dated sample from CE11_05 contained older material either resulting from the heavy bioturbation evident on the X-ray images or because the top of the sandy layer that forms the cap to the debrite was not completely avoided when sampling; (2) the top 1 meter of the core is significantly compressed. However, the shape of the trace fossils does not suggest any significant compression, so this possible interpretation is ruled out; (3) sediment was preferentially depositing where there was more accommodation space, and CE11_06 was taken from inside a scar, whereas CE11_05 just outside it. The elevation difference between the two cores is 65 m.

4.5. Evidence of Separate Slide Events and Estimated Volumes Involved

The new high-resolution air gun data have revealed the distribution of the slide deposits (facies 4), and the facies between them that allows the identification of at least three episodes of slope instability. We assume that the geometry of each of the individual buried failure deposits is lobate in shape with a NW-SE axis, similar to the lobes evident on the seafloor surface, in order to estimate their volume and areal extent in the absence of a denser network of seismic lines. On the basis of the seismic profiles, three distinct slide deposits can be identified (slides A, B, and C; Figure 4).

Slide A is found in the deepest section (between reflectors R2 and R3), separated vertically by about 10-ms-thick hemipelagic sediments (facies 1 and/or 5) from slide deposits B1, B2, and C (Figure 4). The slide deposits vary in thickness from 70 ms down to below the limit of resolution (10 ms) and have an average thickness of 30 ms. Using an acoustic velocity of 1,700 m/s for moderately consolidated sediments (Hamilton & Bachman, 1982), this corresponds to slightly less than 30 m. The area the Slide A deposits occupy is estimated at about 7,500 km^2 (Figure 9) indicating an approximate volume of approximately 225/km

Slide B comprises two parts (B1 and B2) that are highly erosive, judging by the thickness of truncated sediments against the edges of the deposits. B1 and B2 are separated laterally by a segment of undisturbed seafloor sediments (Figure 4b). While they may indicate two separate slide events, they are found at the same

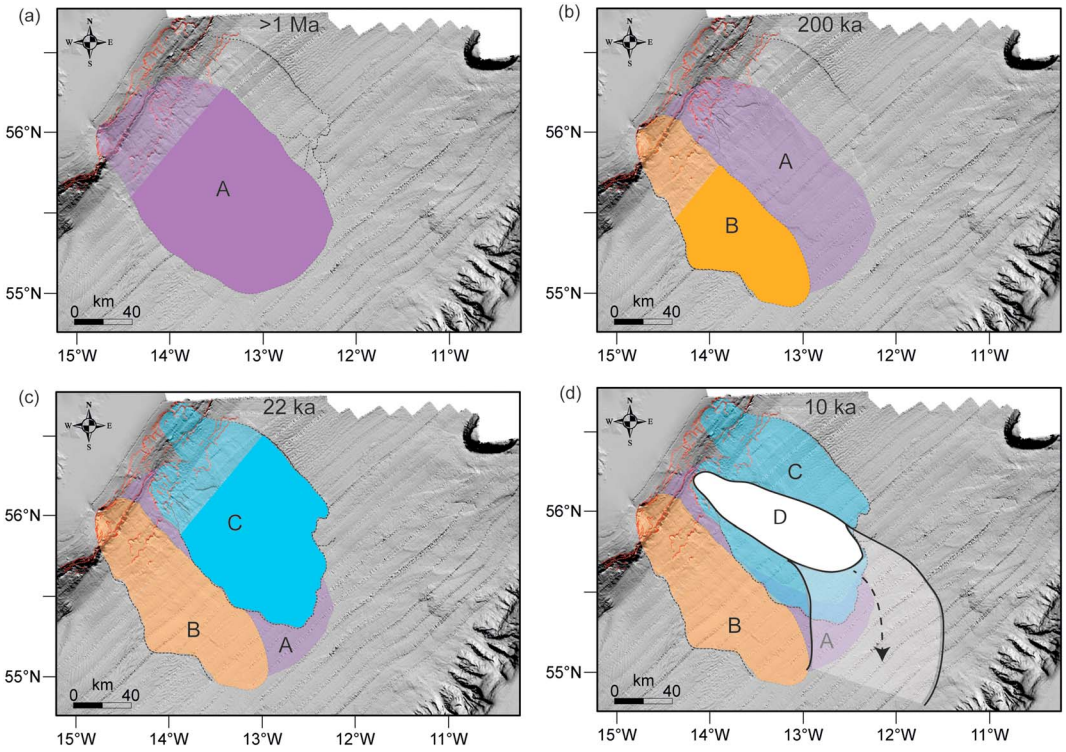

Figure 9. (a–d) Inferred distribution of Slides A, B, C, and D based on the seismic and core data as well as the seafloor lobes as expressed on the bathymetry, in the order they took place. The lighter shaded area is the interpreted evacuation area, whereas the darker shaded area is the interpreted depositional area (for each panel the entire area of the earlier slides is lightly shaded). The arrow in (d) indicates the direction of flow of the Slide D turbidity current, and the transparent white area indicates the extent to which it spread.

stratigraphic level. This favors an interpretation where B1 and B2 are part of the same event that bifurcates around a remnant seafloor block or rafted block. Interestingly, we observe a similar pinnacle-like feature on the seafloor vertically above the remnant seafloor block (Figure 4b). This pinnacle in fact corresponds to an elongate ridge that strikes parallel to the flow direction. It is therefore likely that a similar ridge caused Slide B to bifurcate around it. Slide B is 20–60 ms thick, on average 35 ms, which with an acoustic velocity of 1,600 m/s for less consolidated sediments than Slide A (Hamilton & Bachman, 1982) as this is at shallower stratigraphic level, corresponds to ~30-m thickness. The extent of Slide B is more limited than slide A, at 4,500 km^2, and we estimate the volume to be ca 125 km^3.

Slide C is characterized by variable internal acoustic character, probably due to different degrees of disintegration and potentially variable lithology (Figure 4). This deposit is thicker than slide B, at about 120-ms maximum thickness but has an average thickness of 75 ms, or 60 m (assuming the same acoustic velocity of 1,600 m/s as for slide B). The cores sample the top part of this deposit but do not penetrate it fully (orange line in Figures 7 and 8 marks the top of the deposit); Slide C is linked with the lobes that extend on the seafloor downslope of the North Upper Slope scar and the Lower Slope scar (after Georgiopoulou et al., 2013), and we calculate its extent at 6,600 km^2 (Figure 9) and its volume at approximately 400 km^3, making Slide C the most voluminous of the three slides.

A fourth event, Slide D, is only identifiable in the cores as it is too thin to be resolved by the seismic data (purple line in Figures 7 and 8). In some cores we only observe a fining upward turbidite (medium to fine sand; e.g., cores 08/09_sc1, CE14_13A), while in others the turbidite caps a clast-supported debrite (facies CD; e.g., cores CE14_07A, CE14_06A, and possibly CE14_08B). It occupies the central downslope area according to its distribution in the cores (Figure 9d). Its deposits suggest that it was a dilute event (further discussion in section 5.1) that generated a turbidity current, which flowed ESE and was directed southeastward toward the deepest part of the Rockall Trough, following the seafloor topography (Figure 9). The average thickness of the event in the study area is 30 cm, and it occupies an area of 4,000 km^2, which gives a volume of at least

1.2 km^3. The volume of the turbidite, which is on average 10 cm thick and occupies an area of nearly 5,000 km^2, adds another 0.5 km^3.

The volume of the RBSC was previously calculated by Georgiopoulou et al. (2013) based on estimates of the missing sediments from the scars on the Rockall Bank slope. They used two approaches: a *conservative* approach, where the volume of evacuated sediments was based on connecting the scarps by straight, planar surfaces, and a more *generous* approach, where the volume of evacuated sediments was calculated by connecting the scarps with dome-shaped surfaces. The two approaches generated volumes that vary from 265 to 765 km^3 of missing sediments. The present study indicates the total volume of the four slide deposits amounts to approximately 750 km^3, which is very close to the generous volume of Georgiopoulou et al. (2013). This also suggests that the generous approach, where a mounded contouritic morphology on the Rockall Bank slope was considered prior to slope collapse, is more realistic than the conservative approach in estimating the missing volumes from the scars. However, it should be noted that one of the slides, Slide B, was highly erosive (as discussed above), and therefore, the volume of the deposits should exceed the volume of the evacuated sediments, but it is difficult to estimate by how much.

4.6. Emplacement Age of RBSC Events

We have calculated a sedimentation rate of about 12 cm/ka for the last 20 ka for the Rockall Bank slope and about 2.5 cm/ka for the deeper Rockall Trough, away from the influence of bottom currents (Table 1). In order to estimate the ages of the older events we have extrapolated the Rockall Bank sedimentation rate back, assuming constant sedimentation rates and recognizing the uncertainties and potential errors in this approach, particularly the deeper in the record we extrapolate where climatic changes would have affected sedimentation rates significantly. In addition we are considering average radiocarbon ages rather than ranges, which also contain errors.

Slide A is the oldest event. It is difficult to estimate its age with any confidence as there is no way of knowing how much sediment has been removed through erosion by Slides B and C that overlie it. All we can say confidently about Slide A is that it is older than horizon R3, which is probably a few Ma old given the thickness of acoustic facies 5 and the sedimentation rate we have calculated and employed. However, it would be unreasonable to use the same sedimentation rate for the length of period it would have taken to deposit this amount of sediment considering how variable sedimentation rate can be over time.

The southernmost deposit, Slide B, is buried under approximately 24 m of sediments, which with the above sedimentation rate for the Rockall Bank slope (12 cm/ka), yields an estimated age of 200 ka.

Slide C appears to have deposited at approximately the same stratigraphic level as Slide B, on top of Horizon R2 and adjacent to Slide B (Figure 4b), probably due to the seafloor topography that Slide B created and then Slide C was routed through it. However, Slide C appears on seismic profiles to be either exposed at the seafloor (Figure 4) or if there is a drape on it, it is thinner than the vertical seismic resolution (approximately 8 m). By assuming a drape thinner than 8 m and using a sedimentation rate of 12 cm/ka we can estimate that Slide C is younger than approximately 70 ka. A subbottom profile shown in Georgiopoulou et al. (2013; their Figure 5) shows recent slide deposits inside the Upper North Slide scar, upslope of Slide C. Their results indicate that either Slide C is actually significantly younger than 70 ka or that there has been another, very recent slope collapse in the same area that is not resolved on the seismic data. Indeed, even high-resolution Pinger data with 1-m vertical resolution do not show slope collapses in the area younger than Slide C (Sacchetti, Benetti, Quinn, et al., 2012, see their Figure 5). However, our core data clearly demonstrate that there has been a more recent failure, Slide D, that was deposited only about 0.5 m above Slide C and therefore could not be resolved even by the pinger high-resolution data (Figures 7a and 8). The only way to distinguish and establish the distribution of Slides C and D is based on the presence (or absence) of the youngest event in the cores.

Core CE11_02 suggests that there has been an event, at 20,850 calibrated (cal) BP (which is the age of the sample taken 35 cm above the top of the debrite, 17,940 cal BP, plus the 2910 years that it would have taken to deposit the 35 cm at 12 cm/ka sedimentation rate). This 20,850 cal BP event is not found in CE11_01, which was collected from the undisturbed seafloor adjacent to the slide side scarp to the north. The event is found in CE11_06 where it has a very similar age of 21,750 cal BP. The sandy turbidite that caps the debrite in CE11_06 is also found in CE11_05, although the age in core CE11_05 suggests that this layer of sand is

older (28,540 cal BP), which would make them uncorrelated. However, this sample was taken from a part of the core that appears to be heavily bioturbated (Figure 7a), which could have mixed in older material. We suggest that this is the same sandy layer based on its stratigraphic position downcore and the physical properties (Figure 7a). We considered whether the sandy layer in CE11_04, between sections 1 and 2, also correlated with the sandy layer in CE11_05 and CE11_06, but the physical properties and mineralogy differ (Figure 7a); in CE11_05 and CE11_06 the sand is foraminifera-dominated and contains rounded and angular lithic grains, whereas in CE11_04 there are very few foraminifera relative to the clastic material, which is dominated by glassy angular quartz and dark green lithic fragments. There are also significant differences in the physical properties; crucially, the magnetic susceptibility that is a reflection of mineralogy is higher in CE11_05 and CE11_06, whereas the *P* wave velocity and gamma-ray density are higher in CE11_04. Therefore, we do not believe that the sandy layer correlates across into CE11_04. Core CE14_12 contains a debrite capped by a very thin sand layer dated at 22,037 cal BP, which correlates well with the other cores. The same event appears in core 09/07_sc1, dated at 21,744 ka (Øvrebø et al., 2005), which is also in very close agreement with the other ages and with an error range that makes them overlap. Cores CE11_03 and CE11_04 contain no debrites at the appropriate stratigraphic interval, but the sedimentary sequence from about 1 m downcore, which is where a Slide C deposit would have been anticipated, appears disturbed in CE11_03. This could have resulted from slide material buttressing against and plowing through the seafloor further upslope and causing in situ deformation of the seafloor. Alternatively, it could be due to the coring procedure, which is not uncommon with piston coring (Jutzeler et al., 2014), but the deformation we see in this interval does not match any of the previously described types; that is, it is not limited to the sandy intervals; there is no arcuate warping of the layers or extension and breaking of the muddy interval. Instead, the deformation is consistent with plastic deformation of soft sediments as it would appear in a debrite only the stratigraphic order of the layers has not been altered. As seen on the bathymetric data, cores CE11_03 and CE11_04 were taken from the edges of depositional lobes of Slide C, that is, very close to causes of seafloor disturbance. Based on the correlation of the sandy turbidite layer across CE11_05 and CE11_06, it appears that the 22-ka event that generated the debrite/turbidite seen in CE11_05 and CE11_06 may have been responsible for the deformation seen in CE11_03. A similar character is observed at a similar stratigraphic position in core CE14_14 that was taken from the edge of the lobe on the southern side of the complex (Figure 7a). The 08/02_sc1 does not have a deposit that correlates with this event. Nevertheless, there is a very sharp contact between contrastingly different hemipelagic sediments (on the basis of color and lithology; Figure 7a). This surface could only have been created by an erosional event and given its stratigraphic position we assign it to the 22-ka event. Given the coincidence of the distribution of the debrite/turbidite in the cores and the distribution of Slide C on the seismic, we believe that Slide C is the 22-ka event.

Across the cores from the Lower slope region and in the middle of the slide complex we found a younger debrite-turbidite pair higher in the stratigraphy (Slide D). This event is encountered in cores CE14_13A (dated 8,760 cal BP) and CE14_07A (dated 9,120 cal BP), in 08/09_sc1 (dated 10,202 cal BP) from Øvrebø et al. (2005), and possibly in CE11_03 as a thin turbidite, without a debrite. The age of this event has been determined to be around 10 ka. The absence of this deposit from CE11_05, CE11_06, 08/01_sc1, and 08/02_sc1 (Figure 8) suggests that this flow followed a narrow ESE trajectory. This event coincides stratigraphically with the T2 turbidite described by Georgiopoulou et al. (2012) in the deeper Rockall Trough.

There appears to be a recent debrite near the top of CE14_07A as well as the top of 78/30_sc1 and a turbidite at the top of CE14_06A, while the entire CE14_08B consists of a debrite deposit capped by a turbidite that is at the top of the core. It is hard to determine whether the deposits in CE14_08B and 78/30_sc1 correlate with the 10-ka event or the even more recent event. This latest event does not have a large extent and is not identified in cores further away from the scarps, so it is likely that it is the result of scarp spalling and small equilibrium adjustments (e.g., (Carter et al., 2018)).

5. Discussion

5.1. Styles of Mass Transport

Several different types of deposits have been identified in the RBSC, pointing to a wide range of flows in the spectrum of sedimentary flow processes, from dilute to cohesive flows. Core data allow us to

assess and compare the flow processes in the last two phases of slope instability in the RBSC, during Slides C and D.

Slides A and B, being buried deep below the seafloor, and in the absence of their sedimentary record in the cores, cannot be assessed for flow type save for their acoustic record. The top of Slide A appears blocky. However, the large runout and then thinness of the deposit suggest that it must have transformed downslope to a more fluid flow that allowed it to spread laterally.

Similarly, Slide B appears to have been blocky but less widespread and thicker with pronounced and steep lateral margins. From these characteristics we infer that Slide B was probably more concentrated and perhaps flowed more plastically like a debris flow that halted its movement *en masse*, freezing in place. A dilute component that would have deposited a turbidite further downslope cannot be dismissed, but there is no evidence for it with the available data.

Slide C appears to have been a bimodal flow, comprised mostly of a cohesive clast-rich debris flow and an accompanying dilute cloud or tail that deposited a thin turbidite as the flow was waning. The turbidity current could have been either high density or low density as both can deposit laminated sands (Sumner et al., 2012), which is what has been retrieved in the cores. The runout of the turbidity current was not significant, as we do not encounter it in cores beyond the limits of the slide (Georgiopoulou et al., 2012). The top of Slide C appears smoother than Slides A and B, and we interpret this to mean that the character of this flow was less blocky and maybe more plastic. Similar to slide B, the toe of Slide C appears thick, thicker than the body of the slide (Figure 4), and set within stratified preexisting sediments as if it buried and confined itself, plowing through the seafloor. Small-scale thrusts are likely present at the toe (Figure 4) lending further evidence toward a self-confining type of flow but not to the extent previously reported for self-confining submarine landslides (Frey Martinez et al., 2005). Further corroborating evidence comes in the form of the sheared section in core CE11_03 that appears as though in situ layers have been locally deformed, possibly due to the lateral pressures emanating from the toe of the slide plowing through the adjacent seafloor. Different scenarios for modeling of Slide C to match the deposits as seen on the bathymetric data reveal that the best fit resulted when a Bigham rheology was adopted with either a velocity-dependent term or with basal frictional properties (Salmanidou et al., 2018).

Slide D, on the other hand, appears to have been more dilute, perhaps fully transformed into a turbidity current as indicated by the deposit found in the cores. However, in spite of its dilute nature, this flow did not spread laterally much but did have a long runout and extended mostly downslope as it can be found in a deeper part of the basin (Georgiopoulou et al., 2012). These characteristics suggest that Slide D was more rapid and more focused than the previous episodes of failures as it is found along a relatively narrow, elongate axis (Figure 9d).

Finally, the latest episode was probably generated by minor secondary scarp spalling that did not produce a large event, and the deposits have not gone far from the scarp source. The timing of this event is estimated to be some time in the last millennium as there does not seem to be any substantial drape covering it.

The sequence of events described here based on the depositional data is in general agreement with the sequence of events proposed by Georgiopoulou et al. (2013). However, the present study reveals that these events took place over a considerable period of time. This has also demonstrated the predisposition of the slope for ongoing slope instability and repetitive failure. For example, Slides A and B appear to originate from the same source, even though Slide B was almost half the size of A, but it may have resulted from retrogression of the Slide A scarp.

Attempts to model the flow behavior of Slides A and B, using the same approach as for slide C, demonstrated that this was not possible and the modeled deposits mapped beyond the actual ones (Salmanidou et al., 2018). This was attributed to potentially different rheological properties (Salmanidou et al., 2018). Therefore, the assumption that slide events that occur in the same area and as a result should have the same lithological characteristics, and by extension rheological characteristics, is wrong, at least for this case study, as demonstrated by Salmanidou et al. (2018) and by the different deposits we find in the cores in this study.

We also observe that slide events become more frequent in more recent geological time. This does not necessarily reflect an increased rate of slope failure but is more likely a reflection of the increased resolution closer to the seafloor. This could indicate that the thick deposits identified in the deeply buried slides may

comprise the composite products of a number of smaller stacked events rather than the result of single large events.

5.2. Wider Implications

Early work suggested that the RBSC probably occurred as a single event (Faugères et al., 1981; Flood et al., 1979). Georgiopoulou et al. (2013) examined the scarp morphology at the headwall of the complex and suggested that there may have been several episodes given that the *freshness* or angularity of the scarps varies across the slope, but they were unable to draw any conclusions regarding the timing of events, other than that there were likely to have been significant hiatuses between events as seafloor modifications and healing appeared to have taken place over the older events.

In this study, with access to new high-resolution seismic data and a large number of new cores from the depositional area, we are able to confirm the multistage nature of RBSC and cast new light on the emplacement ages and timing between separate events. We are thus able to demonstrate the long history of instability of the Rockall Bank eastern slope. The youngest slide event that appears at the top of a limited number of cores likely took place within the last 1,000 years, but it appears that it was very small and did not affect a significant area. The 10-ka event (Slide D) was a relatively small event in terms of volume (<2 km^3) but had a very long runout. Slide D was nowhere near as voluminous as Slides A, B, and C, but it is significant nonetheless and demonstrates that more events of these dimensions may be hidden in the resolution of the seismic data, which has implications for risk assessment studies that consider the repeat interval of submarine slope failures.

The youngest of the large events (Slide C) appears to coincide with the Last Glacial Maximum, the height of the last glaciation (Clark et al., 2012). During glacial periods, when the sea level fell, continental margins experienced increased terrigenous input as much of the shelf was exposed and became a sediment source (Johannessen & Steel, 2005). A lower sea level may have exposed part of the Rockall Plateau as a small island, but it could not have been large enough to generate the required large amounts of sediment input as it is not connected to a landmass and its dimensions are limited. Additionally, the predominant sediment supply for Rockall Bank, as evidenced by seismic profiles and cores, came through bottom currents running parallel to the slope (Georgiopoulou et al., 2013; O'Reilly et al., 2005; Øvrebø et al., 2005; Stoker et al., 2005). However, bottom currents in Rockall Trough are considered to have been slow during glacial times, with seafloor sediment waves barely affected and with minimum winnowing power (Howe, 1996). Previous studies have suggested a combination of rapid sediment accumulation from bottom currents on top of steep basement scarps and slope undercutting by the bottom currents as instability triggering mechanism for this slope (Elliott et al., 2010; Georgiopoulou et al., 2013). However, given the timing of Slide C at 22 ka, could this mechanism have been a primary trigger? It is likely that the slope reacted with some lag time and currents had already destabilized it prior to their weakening and a ground vibration acted as the final trigger. Another factor that may have contributed is fluid seepage to the seafloor. A number of closely spaced faults can be seen in the seismic profiles (Figure 4a) that may have also facilitated fluid flow to the seafloor, but no direct evidence for fluid seepage can be seen on this resolution of seismic or the bathymetry.

At 22 ka the BIIS was starting to decline (Clark et al., 2012). Models of isostatic loading for the Eurasian Ice Sheet that includes the BIIS show that isostatic loading did not affect Rockall Bank (Patton et al., 2016) that lies just at the limit of the affected region (see Figure 12 of Patton et al., 2016). Isostatic unloading readjustment is experienced in an extensive area beyond the center of the ice load, which is about 10° of longitude (roughly 1,000 km) for the BIIS-sized ice load (Lambeck, 1996). The affected area on Rockall Bank lies a few kilometers inboard of this radius (Figure 10). During that time (22 ka), the ice sheet was still very close to its maximum extent, still occupying the Irish Shelf (Peters et al., 2016), that is, most of the ice load was still in place. Models based on relative sea level data from around Ireland and Scotland show that deglaciation was very rapid *after* 21 ka (Brooks et al., 2008). Therefore, seismicity due to isostatic rebound as the cause of the 22-ka Rockall Bank slope failure is unlikely. Therefore, we conclude that the generation of the 22-ka slope failure event (slide C) was most probably unrelated to the climatic conditions. However, seismicity, unrelated to isostatic rebound, may have well been responsible for Slide C, even though the area is not generally very active seismically (Figure 10).

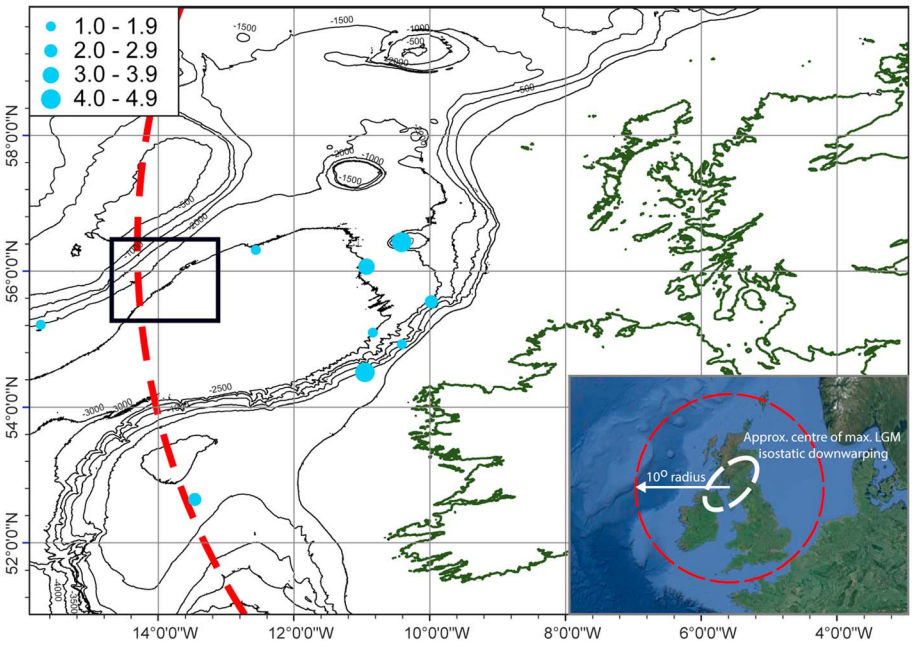

Figure 10. Location of study area (black box) relative to the extent of the area affected by isostatic downwarping (red dashed line) according to Lambeck (1996). Also shown are earthquake magnitudes since 1980 (from the Irish National Seismic Network).

Seismicity due to isostatic rebound may have been responsible for Slide D and for the more recent event. The initiation area for Slide D is also within the area of influence of the main sweeping bottom current in the area that is strong enough to incise a moat at the base of slope of Rockall Bank.

Slide C was modeled by Salmanidou et al. (2017), and it was shown to have generated a 5- to 10 m-high tsunami that traversed Rockall Trough and impacted on the Co. Mayo coast, NW Ireland. However, given the timing, it is unlikely it reached the coast, having encountered the BIIS first, which at 22 ka was still occupying the Irish shelf (Clark et al., 2012; Peters et al., 2016; Sacchetti, Benetti, Quinn, et al., 2012). The ice shelf would likely have dampened the effect of the tsunami wave. Although the question of whether or not Slides C or D could have generated tsunamis is beyond the scope of the present project, it is a topic worthy of further study as the affected slope has not been fully evacuated and potential incipient scarps can be seen on the seafloor (Georgiopoulou et al., 2013; and their Figure 6), and at least one, albeit much smaller event has taken place following Slides C and D.

For tsunami risk assessments it is imperative that studies like the current one are undertaken prior to modeling, in order to separate and distinguish the different events that constitute a slide complex; otherwise, the risk may be overestimated or even underestimated. Very large events (several hundreds of cubic kilometers) that would generate more destructive tsunamis tend to have large recurrence intervals and therefore, while the hazard exists, the risk may be considered small. However, smaller and medium scale landslides (tens to a few hundreds of cubic kilometers) will have shorter recurrence intervals and therefore the risk increases. Other factors such as sedimentation rates and slope replenishment should also be considered when assessing risk of future slide events.

This study has demonstrated that (a) it is more likely that large buried slide events comprise multiple smaller stacked events; (b) slide-prone areas can fail repeatedly along the same scarps or regions, so these areas are at risk of failing again in the future; and (c) slide events originating on the same slope, with the same sediment source, may have very different flow behavior probably because each slide creates new conditions for the slope and the seafloor that gets traversed by the following slide. Perhaps the later slides tap into different lithologies or even remobilize earlier slide deposits, which, in combination with the changed topography and the increased bed roughness, may have significant effects in determining the flow behavior, allowing younger slides to disaggregate more, complicating further forecasting future slide behaviors and tsunami modeling.

6. Conclusions

Using a set of newly acquired high-resolution seismic profiles and gravity cores from the depositional area of the RBSC, we have been able to demonstrate that the following:

1. The complex comprises at least three large-scale slides of 200, 125, and 400 km^3 each, Slides A, B, and C in order of occurrence from oldest to youngest.
2. Slides A and B occupy the southernmost part of the complex, while Slide C extends across the middle and northernmost parts. This suggests that different parts of the slope were unstable, although the southern scarp appears to have been unstable on at least two occasions.
3. The most recent events, Slides C and D and the small local event, are dated at 22 ka, 10 ka, and within the last 1,000 years, respectively.
4. Based on the three most recent events, the recurrence period for slope instability in Rockall Bank is about 10 ka, although this is based on only three data points and should be taken with caution.
5. The repeated instability focused on this part of the Rockall bank slope over such a long period of time suggests that slope instability conditions are persistent through time and that may indicate that this slope is inherently unstable.
6. The concurrence of Slide C with the beginning of deglaciation of the BIIS appears to be coincidental.
7. Multiple events from the same source area can and do generate events with different flow behaviors.

Acknowledgments

Bathymetric data used in this paper can be found on www.infomar.ie. New core raw data (core descriptions and MSCL measurements) and all CE11011 seismic profiles are provided as supporting information. Other cores used are published in literature. This study has been supported by the Irish National Development Plan Marine Research Sub-Programme. We wish to express our gratitude to the Officers, Scientists and Crew of Celtic Explorer expeditions CE11011 and CE14011 for all the help and good times. A. G. would like to acknowledge the Griffith Geoscience Awards and the Geological Survey Ireland Short Call awards (grant 2015-sc-036). Seismic data collection was supported by the Deutsche Forschungsgemeinschaft (grant KR2222/14-1). We are grateful to the reviewers Alexandre Normandeau, Maureen Walton, and Alexey Portnov for their constructive comments.

References

Brooks, A. J., Bradley, S. L., Edwards, R. L., Milne, G. A., Horton, B., & Shennan, I. (2008). Postglacial relative sea-level observations from Ireland and their role in glacial rebound modelling. *Journal of Quaternary Science*, *23*(2), 175–192. https://doi.org/10.1002/jqs.1119

Bull, S., Cartwright, J., & Huuse, M. (2009). A review of kinematic indicators from mass-transport complexes using 3D seismic data. *Marine and Petroleum Geology*, *26*(7), 1132–1151. https://doi.org/10.1016/j.marpetgeo.2008.09.011

Carter, G. D. O., Huvenne, V. A. I., Gales, J. A., Lo Iacono, C., Marsh, L., Ougier-Simonin, A., et al. (2018). Ongoing evolution of submarine canyon rockwalls; examples from the Whittard Canyon, Celtic Margin (NE Atlantic). *Progress in Oceanography*, *169*, 79–88. https://doi.org/10.1016/j.pocean.2018.02.001

Clark, C. D., Hughes, A. L. C., Greenwood, S. L., Jordan, C., & Sejrup, H. P. (2012). Pattern and timing of retreat of the last British-Irish Ice Sheet. *Quaternary Science Reviews*, *44*(0), 112–146. https://doi.org/10.1016/j.quascirev.2010.07.019

Elliott, G. M., Shannon, P. M., Haughton, P. D. W., & Øvrebø, L. K. (2010). The Rockall Bank mass flow: Collapse of a moated contourite drift onlapping the eastern flank of Rockall Bank, west of Ireland. *Marine and Petroleum Geology*, *27*(1), 92–107. https://doi.org/10.1016/j.marpetgeo.2009.07.006

Faugères, J. C., Gonthier, E., Grousset, F., & Poutiers, J. (1981). The Feni Drift: The importance and meaning of slump deposits on the eastern slope of the Rockall Bank. *Marine Geology*, *40*(3-4), M49–M57. https://doi.org/10.1016/0025-3227(81)90138-9

Faugères, J. C., Stow, D. A. V., Imbert, P., & Viana, A. (1999). Seismic features diagnostic of contourite drifts. *Marine Geology*, *162*(1), 1–38. https://doi.org/10.1016/S0025-3227(99)00068-7

Flood, R. D., Hollister, C. D., & Lonsdale, P. (1979). Disruption of the Feni sediment drift by debris flows from Rockall Bank. *Marine Geology*, *32*(3–4), 311–334. https://doi.org/10.1016/0025-3227(79)90070-7

Frey Martinez, J., Cartwright, J., & Hall, B. (2005). 3D seismic interpretation of slump complexes: Examples from the continental margin of Israel. *Basin Research*, *17*(1), 83–108. https://doi.org/10.1111/j.1365-2117.2005.00255.x

Georgiopoulou, A., Benetti, S., Jones, S. M., & Wall, D. (2010). RV Celtic Explorer CE10008, 3rd - 17th June, 2010 (Galway-Galway): Glacial and non-glacial sediment transport and seismic oceanography in the Rockall Trough, NE Atlantic *Rep*, 24 pp, Marine Institute, Galway.

Georgiopoulou, A., Benetti, S., Shannon, P. M., Haughton, P. D. W., & McCarron, S. (2012). Gravity flow deposits in the deep Rockall Trough, Northeast Atlantic. In Y. Yamada, et al. (Eds.), *Submarine mass movements and their consequences, Advances in Natural and Technological Hazards Research*, (pp. 695–707). Dordrecht Heidelberg London New York: Springer.

Georgiopoulou, A., Shannon, P. M., Sacchetti, F., Haughton, P. D. W., & Benetti, S. (2013). Basement-controlled multiple slope collapses, Rockall Bank slide complex, NE Atlantic. *Marine Geology*, *336*, 198–214. https://doi.org/10.1016/j.margeo.2012.12.003

Hamilton, E. L., & Bachman, R. T. (1982). Sound velocity and related properties of marine sediments. *The Journal of the Acoustical Society of America*, *72*(6), 1891–1904. https://doi.org/10.1121/1.388539

Harkness, D. (1983). The extent of the natural ^{14}C deficiency in the coastal environment of the United Kingdom, *Proceedings of the First International Symposium 14C and Archaeology*, PACT 8, 351–364.

Holmes, R., Long, D., & Dodd, L. R. (1998). Large-scale debrites and submarine landslides on the Barra Fan, west of Britain. *Geological Society, London, Special Publications*, *129*(1), 67–79. https://doi.org/10.1144/GSL.SP.1998.129.01.05

Howe, J. A. (1996). Turbidite and contourite sediment waves in the northern Rockall trough, North Atlantic Ocean. *Sedimentology*, *43*(2), 219–234. https://doi.org/10.1046/j.1365-3091.1996.d01-1.x

Hunt, J. E., Wynn, R. B., Masson, D. G., Talling, P. J., & Teagle, D. A. H. (2011). Sedimentological and geochemical evidence for multistage failure of volcanic island landslides: A case study from Icod landslide on North Tenerife, Canary Islands. *Geochemistry, Geophysics, Geosystems*, *12*, Q12007. https://doi.org/10.1029/2011GC003740

Johannessen, E. P., & Steel, R. J. (2005). Shelf-margin clinoforms and prediction of deepwater sands. *Basin Research*, *17*(4), 521–550. https://doi.org/10.1111/j.1365-2117.2005.00278.x

Jutzeler, M., White, J. D. L., Talling, P. J., McCanta, M., Morgan, S., Le Friant, A., & Ishizuka, O. (2014). Coring disturbances in IODP piston cores with implications for offshore record of volcanic events and the Missoula megafloods. *Geochemistry, Geophysics, Geosystems*, *15*, 3572–3590. https://doi.org/10.1002/2014GC005447

Lambeck, K. (1996). Glaciation and sea-level change for Ireland and the Irish Sea since Late Devensian/Midlandian time. *Journal of the Geological Society, London*, *153*(6), 853–872. https://doi.org/10.1144/gsjgs.153.6.0853

O'Reilly, B. M., Readman, P. W., & Shannon, P. M. (2005). Slope failure, mass flow and bottom current processes in the Rockall Trough, offshore Ireland, revealed by deep-tow sidescan sonar. *First Break*, *23*, 45–50.

O'Reilly, B. M., Shannon, P. M., & Readman, P. W. (2007). Shelf to slope sedimentation processes and the impact of Plio-Pleistocene glaciations in the Northeast Atlantic, west of Ireland. *Marine Geology*, *238*(1–4), 21–44. https://doi.org/10.1016/j.margeo.2006.12.008

Øvrebø, L. K., Haughton, P. D. W., & Shannon, P. M. (2005). Temporal and spatial variations in late Quaternary slope sedimentation along the undersupplied margins of the Rockall Trough, offshore west Ireland. *Norwegian Journal of Geology*, *85*, 279–294.

Patton, H., Hubbard, A., Andreassen, K., Winsborrow, M., & Stroeven, A. P. (2016). The build-up, configuration, and dynamical sensitivity of the Eurasian ice-sheet complex to Late Weichselian climatic and oceanic forcing. *Quaternary Science Reviews*, *153*, 97–121. https://doi.org/10.1016/j.quascirev.2016.10.009

Peters, J. L., Benetti, S., Dunlop, P., Cofaigh, C. Ó., Moreton, S. G., Wheeler, A. J., & Clark, C. D. (2016). Sedimentology and chronology of the advance and retreat of the last British-Irish Ice Sheet on the continental shelf west of Ireland. *Quaternary Science Reviews*, *140*, 101–124. https://doi.org/10.1016/j.quascirev.2016.03.012

Reimer, P., Bard, E., Bayliss, A., Beck, J., Blackwell, P., Ramsey, C., et al. (2013). IntCal13 and Marine13 Radiocarbon Age Calibration Curves 0–50,000 Years cal BP. *Radiocarbon*, *55*(4), 1869–1887. https://doi.org/10.2458/azu_js_rc.55.16947

Sacchetti, F., Benetti, S., Georgiopoulou, A., Dunlop, P., & Quinn, R. (2011). Geomorphology of the Irish Rockall Trough, North Atlantic Ocean, mapped from multibeam bathymetric and backscatter data. *Journal of Maps*, *2011*, 60–81.

Sacchetti, F., Benetti, S., Georgiopoulou, A., Shannon, P. M., O'Reilly, B. M., Dunlop, P., et al. (2012). Deep-water geomorphology of the glaciated Irish margin from high-resolution marine geophysical data. *Marine Geology*, *291-294*(1), 113–131. https://doi.org/10.1016/j.margeo.2011.11.011

Sacchetti, F., Benetti, S., Quinn, R., & Cofaigh, C. Ó. (2012). Glacial and post-glacial sedimentary processes in the Irish Rockall Trough from an integrated acoustic analysis of near-seabed sediments. *Geo-Marine Letters*, *33*(1), 49–66.

Salmanidou, D. M., Georgiopoulou, A., Guillas, S., & Dias, F. (2018). Rheological considerations for the modelling of submarine sliding at Rockall Bank, NE Atlantic Ocean. *Physics of Fluids*, *30*(3), 030705. https://doi.org/10.1063/1.5009552

Salmanidou, D. M., Guillas, S., Georgiopoulou, A., & Dias, F. (2017). Statistical emulation of landslide-induced tsunamis at the Rockall Bank, NE Atlantic. *Proceedings of the Royal Society A: Mathematical, Physical and Engineering Sciences*, *473*, 20170026. https://doi.org/10.1098/rspa.2017.0026

Stoker, M. S. (1998). Sediment-drift development on the continental margin off NW Britain. In M. S. Stoker, D. Evans, & A. Cramp (Eds.), *Geological processes on continental margins: Sedimentation, mass-wasting and stability*, (pp. 229–254). London: Geological Society Special Publication.

Stoker, M. S., Akhurst, M. C., Howe, J. A., & Stow, D. A. V. (1998). Sediment drifts and contourites on the continental margin off Northwest Britain. *Sedimentary Geology*, *115*(1–4), 33–51. https://doi.org/10.1016/S0037-0738(97)00086-9

Stoker, M. S., Praeg, D., Hjelstuen, B. O., Laberg, J. S., Nielsen, T., & Shannon, P. M. (2005). Neogene stratigraphy and the sedimentary and oceanographic development of the NW European Atlantic margin. *Marine and Petroleum Geology*, *22*(9–10), 977–1005. https://doi.org/10.1016/j.marpetgeo.2004.11.007

Stoker, M. S., van Weering, T. C. E., & Svaerdborg, T. (2001). A Mid- to Late Cenozoic tectonostratigraphic framework for the Rockall Trough. In P. M. Shannon, P. D. W. Haughton, & D. V. Corcoran (Eds.), *The petroleum exploration of Ireland's offshore basins* (pp. 411–438). London: Geological Society Special Publication.

Stuiver, M., Reimer, P. J., & Braziunas, T. F. (1998). High-precision radiocarbon age calibration for terrestrial and marine samples. *Radiocarbon*, *40*(3), 1127–1151.

Sumner, E. J., Talling, P. J., Amy, L. A., Wynn, R. B., Stevenson, C. J., & Frenz, M. (2012). Facies architecture of individual basin-plain turbidites: Comparison with existing models and implications for flow processes. *Sedimentology*, *59*(6), 1850–1887. https://doi.org/10.1111/j.1365-3091.2012.01329.x

Unnithan, V., Shannon, P. M., McGrane, K., Readman, P. W., Jacob, A. W. B., Keary, R., & Kenyon, N. H. (2001). Slope instability and sediment redistribution in the Rockall Trough: Constraints from GLORIA. In P. M. Shannon, P. D. W. Haughton, & D. V. Corcoran (Eds.), *The petroleum exploration of Ireland's offshore basins*. London: Geological Society Special Publication.

Ward, S. N., & Day, S. (2001). Cumbre Vieja Volcano-Potential Collapse and tsunami at La Palma, Canary Islands. *Geophysical Research Letters*, *28*(17), 3397–3400. https://doi.org/10.1029/2001GL013110

Weaver, P. P. E., Wynn, R. B., Kenyon, N. H., & Evans, J. (2000). Continental margin sedimentation, with special reference to the north-east Atlantic margin. *Sedimentology*, *47*(Suppl. 1), 239–256. https://doi.org/10.1046/j.1365-3091.2000.0470s1239.x

van Weering, T. C. E., & de Rijk, S. (1991). Sedimentation and climate-induced sediments on Feni Ridge, Northeast Atlantic Ocean. *Marine Geology*, *101*(1–4), 49–69. https://doi.org/10.1016/0025-3227(91)90062-9

Wynn, R. B., & Stow, D. A. V. (2002). Classification and characterisation of deep-water sediment waves. *Marine Geology*, *192*(1–3), 7–22. https://doi.org/10.1016/S0025-3227(02)00547-9